Article

Hyphenation of Field-Flow Fractionation and Magnetic Particle Spectroscopy

Norbert Löwa [1,2,*], Patricia Radon [1], Dirk Gutkelch [1], Rinaldo August [2] and Frank Wiekhorst [1]

[1] Physikalisch-Technische Bundesanstalt, Abbestr. 2-12, D-10587 Berlin, Germany; E-Mails: patricia.radon@ptb.de (P.R.); dirk.gutkelch@ptb.de (D.G.); frank.wiekhorst@ptb.de (F.W.)

[2] Technische Universität Berlin, Str. des 17. Juni 135, D-10623 Berlin, Germany; E-Mail: norbert.loewa@ptb.de

* Author to whom correspondence should be addressed; E-Mail: norbert.loewa@ptb.de; Tel.: +49-30-3481-7736; Fax: +49-30-3481-7509.

Academic Editor: Ronald Beckett

Abstract: Magnetic nanoparticles (MNPs) exhibit unique magnetic properties making them ideally suited for a variety of biomedical applications. Depending on the desired magnetic effect, MNPs must meet special magnetic requirements which are mainly determined by their structural properties (e.g., size distribution). The hyphenation of chromatographic separation techniques with complementary detectors is capable of providing multidimensional information of submicron particles. Although various methods have already been combined for this approach, so far, no detector for the online magnetic analysis was used. Magnetic particle spectroscopy (MPS) has been proven a straightforward technique for specific quantification and characterization of MNPs. It combines high sensitivity with high temporal resolution; both of these are prerequisites for a successful hyphenation with chromatographic separation. We demonstrate the capability of MPS to specifically detect and characterize MNPs under usually applied asymmetric flow field-flow fractionation (A4F) conditions (flow rates, MNP concentration, different MNP types). To this end MPS has been successfully integrated into an A4F multidetector platform including dynamic ligth scattering (DLS), multi-angle light scattering (MALS) and ultraviolet (UV) detection. Our system allows for rapid and comprehensive characterization of typical MNP samples for the systematic investigation of structure-dependent magnetic properties. This has been demonstrated by magnetic analysis of the commercial magnetic resonance imaging (MRI) contrast agent Ferucarbotran (FER) during hydrodynamic A4F fractionation.

1. Introduction

Nanotechnology holds tremendous potential for new-generation products, materials, and applications in various industrial sectors (e.g., information and communication technology, environment, health care). In the field of medicine and pharmacy, colloidal dispersions of magnetic nanoparticles (MNPs) take a central role as diagnostic and therapeutic tools. They are mainly made of an iron oxide core stabilized by a monomer or polymer shell. Their magnetic properties and low toxicity make them ideally suitable for a broad spectrum of biomedical applications, such as cancer-targeted drug delivery, gene therapy, cell separation, tumor thermoablation, magnetic resonance imaging (MRI), and magnetic particle imaging (MPI) [1–3].

Depending on the desired effect, MNPs must meet particular magnetic requirements which are mainly determined by their size, shape, and crystallographic structure [4]. Further, the structural parameters also substantially influence the behaviour of MNPs in the living organism (biodistribution, biodegradation, clearance) and may be more decisive than the chemical composition of their capping layer or core [5,6]. Therefore, manufacturing as well as quality assurance of MNPs essentially require comprehensive and accurate analytical methods to measure magnetic and structural properties with regard to application performance and risk assessment. This certainly is a challenging task, especially for broad or multimodal distributions of geometric sizes which often arise from common synthetic routes such as coprecipitation [7,8]. Conventional light scattering (LS) techniques, in particular dynamic LS (DLS) and multi-angle LS (MALS), may give misleading information for polydispersed samples by overestimation of average particle size due to the r^6 dependence of the scattering intensity. Aggravating this situation, crystal defects may cause diverging geometric and magnetic sizes (e.g., obtained by direct current magnetometry), making a direct allocation of properties impossible [9].

The family of field-flow fractionation (FFF) techniques is capable to overcome these limitations, offering different physical selection fields to adress particles from 1 nm up to 100 μm [10] under mild operation conditions. The most direct way to assess magnetic properties of MNPs using FFF is to use a magnetic selection field and to apply a sufficient FFF retention theory to extract the magnetic properties. Compared to most types of FFF, the particle properties change with the strength of the applied magnetic field, but this behavior is initially unknown. Further complications may arise from the dipole-dipole interaction of particle magnetic moments, resulting in incomplete fractionation and deviations from theory. Asymmetric flow FFF (A4F) uses a flow field perpendicular to a parabolic laminar flow to separate particles according to different translational diffusion coefficients (D_T) or, rather, hydrodynamic extension. Since A4F provides narrowly distributed particle populations, the main drawbacks of sizing light scattering methods can be circumvented by collecting individual size fractions for subsequent analysis. A more straightforward approach is the simultaneous determination of particle characteristics using hyphenated techniques such as ultraviolet-visible absorbance (UV-vis) for concentration detection, and DLS and MALS for size and shape determination. Though a lot of other analytical techniques have been coupled to FFF [11], so far, no online magnetic characterization

technique has been incorporated. Mainly, this might be due to the fact that known procedures such as direct current magnetometry, linear alternating current (AC) susceptometry, and magnetorelaxometry are either too slow or not sensitive enough within the desired size range. With the invention of MPI in 2005 [12], the nonlinear AC susceptometry, today better known as magnetic particle spectroscopy (MPS), was intensively used to estimate the imaging perfomance of MNPs as it relies on the same physical principle waiving of any spatial encoding. Compared to other magnetic characterization methods, MPS provides a rapid background-free and an extremely sensitive detection of MNPs, making it ideally suitable for chromatographic separations such as A4F. Attempts to develop suitable models for the analysis of MPS signals for the extraction of magnetic parameters are underway and recently of great debate [13-16]. For a comprehensive analysis and higher stability of results, it is recomended to apply different excitation fields B_{exc} or frequencys f_0 [17,18]. It was shown that the combination of A4F with magnetic characterization [19–21], or recently, using offline MPS, enables a more detailed study of size-dependent magnetic characteristics of MNPs [22,23].

This study aims to demonstrate the suitability of MPS to detect and characterize MNPs under prevailing A4F conditions (flow rates, MNP concentration, different MNP types). To this end MPS has been successfully integrated into an A4F multidetector platform including DLS, MALS, and UV. We demonstrate the performance of our system by magnetic analysis of the commercial MRI contrast agent Ferucarbotran (FER) in the run of the hydrodynamic A4F fractionation.

2. Experimental Section

2.1. Samples

The commercial magnetic resonance imaging contrast agent FER (brand name: Resovist®) was purchased from Meito Sangyo (JPN). FER is an aqueous suspension of iron oxide nanoparticles coated with carboxydextran, consisting of single and multi-core MNPs. For A4F 10 µL of MNP were injected in aqueous dispersion at an iron concentration of 0.52 mg/mL which corresponds to 5.2 µg iron. The solvent for A4F was NovaChem100 surfactant (Postnova Analytics GmbH) in a dilution of 0.0125% (v/v) in ultra pure water. For testing the MPS in continuous flow mode not only FER but also starch-coated Fluidmag-D MNPs (FM) purchased from Chemicell (GER) were used (see Table 1).

Table 1. Structural particle parameters of Fluidmag (FM) and Ferucarbotran (FER).

Sample	hydrodynamic size R_{hyd} (nm) [a]	magnetic moment $\mu_m \times 10^{-20}$ (Am²) [b]	saturation magnetization M_s (kA/m)	core type
Ferucarbotran (FER)	26.85(5)	4.2(7) [c]	416(5)	single/multi
Fluidmag-D/30 (FM-30)	14.7(1)	9.8(6)	310(2)	single
Fluidmag-D/50 (FM-50)	30.6(3)	25.8(2)	360(30)	single
Fluidmag-D/100 (FM-100)	64.0(5)	17.9(1)	270(20)	multi
Fluidmag-D/200 (FM-200)	93.5(5)	11.6(1)	380(30)	multi
Fluidmag-D/300 (FM-300)	127(2)	15.0(1)	370(30)	multi

[a] Hydrodynamic size (z-Average) measured by dynamic light scattering (DLS), [b] Effective magnetic moment of individual magnetic nanoparticles (MNPs) determined by direct current (DC) magnetometry according to [24].

[c] Using a bimodal distribution approach according to [25] results in $\mu_{m,1} = 2.8(5)*10^{-20}$ Am² and $\mu_{m,2} = 233(12)*10^{-20}$ Am² with a share of about 30%.

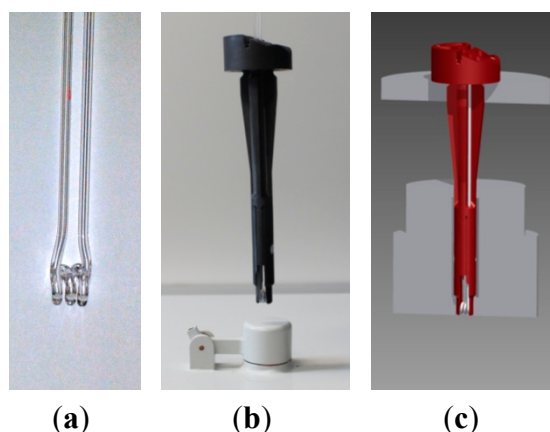## 2.2. Magnetic Particle Spectroscopy (MPS)

The field-dependent magnetization of MNPs is featured by a nonlinear behavior which depends on the particles' magnetic properties. MPS is a sensitive and fast magnetic characterization technique exploiting this special magnetic behavior (nonlinear magnetic susceptibility) of MNPs. We used a commercial magnetic particle spectrometer (Bruker, GER) operating at a sinusoidally varying excitation field with variable field amplitudes in the range B_{exc} = 0.05 mT up to 25 mT (3% accuracy) and a fixed frequency of f_0 = 25 kHz [26]. If MNPs are located in the spectrometer's transmit coil, their magnetization is driven periodically into the nonlinear area of the magnetization curve or beyond into saturation. The induced magnetization response of the MNPs, a deformed sinusoid, is recorded by a receive coil for an adjustable averaging time interval t_{avg} (0.1 s up to 10 s). After filtering to remove the fundamental drive frequency f_0 (excitation), the signal is amplified and Fourier-transformed into the spectrum of harmonics μ_{Ai} at multiples i of the drive frequency f_0. Thus, the deformed response signal of the MNPs is split into its higher harmonic frequency components at odd multiples of the drive frequency f_0. In this study, all measurements were performed at 310 K. To facilitate the comparison of various measured spectra we used the third harmonic amplitude μ_3 (e.g., normalized to the sample's iron content) and the harmonic ratio μ_5/μ_3 as an indicator for the slope of the spectrum.

For MPS measurements in batch mode, PCR tubes capturing 10 µL of sample volume were used. Measured batch mode spectra were corrected for any background signals using the measurement of an empty PCR tube. Continuous flow measurements were performed using a dedicated flow cell (see Section 2.3). Similarly, spectra measured in flow mode were corrected by the subtraction of measurements of a flow cell filled with ultra pure water.

2.3. MPS Continuous Flow Measurements

For measurements in continuous flow, three individual capillary flow cells made of different non-magnetic materials have been developed to be inserted into the receive coil of the MPS spectrometer. The flow cell made of quartz glass, FC2, (see Figure 1a) consisted of a 2.0(5) mm outer diameter and 0.5(2) mm inner diameter capillary glass (HSQ 300, Heraeus, GER) helically coiled (2.5 windings) on the lower end to enlarge the effective volume in the receive coil. For the use of other flexible capillaries (e.g., made of polytetrafluoroethylene, silicone) a mounting was developed and produced by generative manufacturing (FC3L, FC3XL). The guiding of the capillary in the mounting was the same as for the quartz glass flow cell (2.5 windings on the lower end, see Figure 1b,c), again to enlarge the effective volume in the receive coil. Whereas the quartz glass flow cell can be recovered by cleaning with hydrochloric acid, the quick-change mounting for the flexible capillary allows for a simple tube replacement.

The effective volume of the three flow cells in the receive coil of the spectrometer was determined by comparison of 10 µL batch and flow cell measurements using samples (FM, MNPs, and FER) of the same iron concentration (see Table 2). For testing the dependence of the MPS signal on different flow rates, a peristaltic pump (IPC-N, IDEX Healthcare & Science GmbH, GER) was used to circulate the MNPs through the flow cell. The volume of circulation was 1000 µL.

(a) **(b)** **(c)**

Figure 1. Three different flow cells to be used in the MPS spectrometer: (**a**) capillary quartz glass flow cell FC2 with helically coiled lower end. Flow cell with flexible tubing and (**b**,**c**) different effective receive coil volumes FC3L and FC3XL. (**c**) The construction allows for the exact and reproducible positioning of the coiled capillary in axial, transversal, and rotary position. The 2.5 windings in the bottom part of the flow cells are intended to enlarge the effective volume in the receive coil of the spectrometer.

Table 2. Characteristic parameters of three different flow cells for magnetic particle spectroscopy (MPS). The effective volume of the flow cells was determined by comparison of MPS signal intensity obtained from a standard MPS batch (10 µL in PCR tube) with flow cell (entirely filled) measurements. Six different magnetic nanoparticle (MNP) samples were used to calculate the unknown flow cell volume. The uncertainty of the specified volume corresponds to the standard deviation of the six measurements.

Flow cell	Inner diameter (mm)	V_{eff} (µL)	Material
FC2	0.5	10.1(3)	quartz glass
FC3L	0.8	29(1)	polytetrafluoroethylene
FC3XL	1.0	53(2)	silicone

2.4. Asymmetric Flow Field-Flow Fractionation (A4F)

For the fractionation we used a commercial A4F system (Postnova Analytics GmbH, GER). It consists of an AF2000 focus system (manual injection valve, PN7520 inline degasser, PN1130 tip/focus pump). To reduce background signals the solvent was filtered with a 100 nm inline filter directly behind tip and focus pump. The separation channel, with a thickness of 500 µm, was equipped with a regenerated cellulose membrane (with 10 kDa molar weight cut-off) at the accumulation side. To increase the sample concentration, a pulse-free automated stream splitter (PN1650) removed 80% of the eluent from the upper region of the channel just before the sample outlet. The flow program (see Table 3), controlled by the AF2000 software package, was previously optimized according to sample recovery, retention ratio, and selectivity by variation of the cross flow to channel flow ratio V_x/V_{Ch}. Therefore, the ratio V_x/V_{Ch} was varied between 2 and 4 in steps of 0.5 with V_{Ch} remaining constant at 0.5 mL/min (optimum $V_x/V_{Ch} = 3$).

The A4F channel outlet was directly coupled to the UV detector (PN3211, detecting at $\lambda = 280$ nm) followed by the MALS (PN3621, using a light source at $\lambda = 532$ nm), the DLS (Zetasizer NanoZS, Malvern Instruments, UK, using a light source at $\lambda = 633$ nm), and finally the MPS (Bruker, GER) device. The hydrodynamic particle size R_{hyd} was determined from the Stokes-Einstein-Relation for spherical particles $R_h = k_B T/(6\pi\eta D_T)$ with k_B denoting the Boltzmann constant, η the viscosity of the surrounding medium, and T the temperature (295 K), using the apparent diffusion coefficient D_T obtained from DLS. Additionally, nanoparticle sizes were determined by MALS using measured signal intensities at 18 scattering angles ranging from 20° to 156° (steps of 8°). The intensity distribution function assuming spherical particles with a radius R is given by:

$$P(\vartheta) = (\frac{3}{x^3}(\sin x - x\cos x))^2 \tag{1}$$

with

$$x = \frac{R\,4\pi\,n}{\lambda}\sin{^\vartheta/_2} \tag{2}$$

where θ is the observed angle, λ the laser wavelength, P the scattering form factor describing the angular dependence of the intensity of scattered light, and n the refractive index of the solvent medium. As measured intensity distribution profiles agree well with the used model of Equation (1), we consider the approach of spherical particles as valid. To match the detector outputs, the interdetector volume (*i.e.*, time difference) was determined in advance by a calibration run without separation using unfractionated FER of known iron content. Note that the signals were not corrected for potential system contributions to peak broadening caused by detector flow cells, end fittings, and connecting tubing. The calibration run was further used to calibrate the UV signal to directly quantify the iron content in following separations.

Table 3. Asymmetric flow field-flow fractionation (A4F) fractionation parameters.

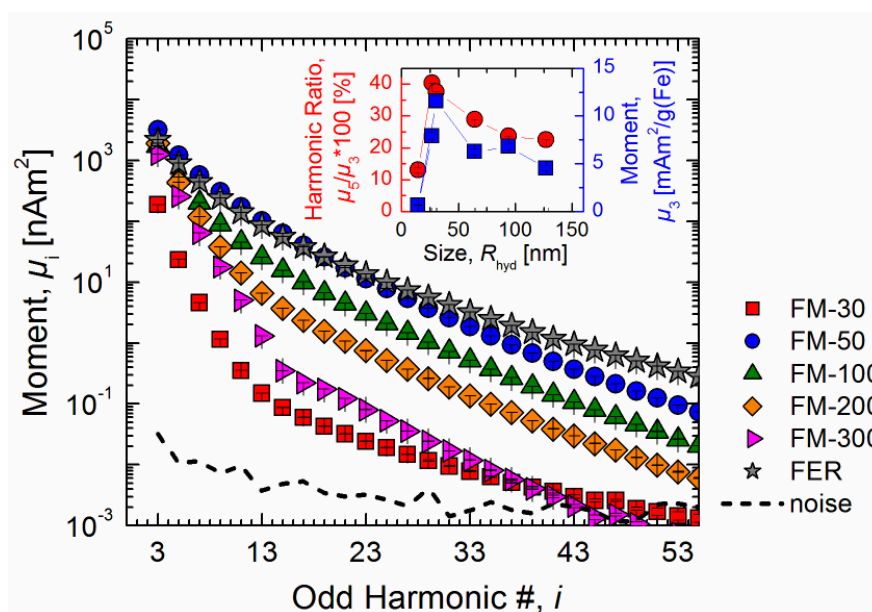| Parameter	Setting
detector flow rate	0.1 mL/min
slot outlet flow rate	0.4 mL/min
cross flow rate	1.5 mL/min (end: 0.1 mL/min)
injection and focusing	4 min
cross flow gradient time	20 min (starting from 14 min elution)

3. Results and Discussion

Preliminary to the online coupling of the A4F multidetector platform with MPS for the simultaneous analysis of MNP size, concentration, and magnetism, the performance of the MPS with respect to sensitivity and applicability under flow conditions was thoroughly tested. The MPS online detection was finally performed using pre-defined appropriate parameters and conditions.

3.1. Influence of MNP Structure

MPS measurements ($B_{exc} = 25$ mT, $t_{avg} = 1$ s) on a set of different MNP types of the same iron concentration ($c(Fe) = 5.6$ mg/mL, $V = 50$ µL) clearly demonstrate that the MNP signal performance is

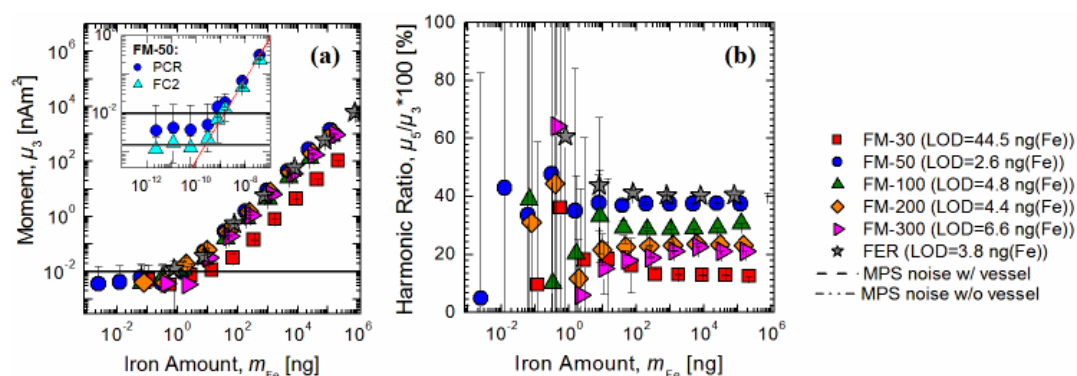strongly affected by differences in structural and magnetic properties (e.g., R_{hyd}, Ms, μ) resulting in rich harmonic spectra with an obviously distinguishable signature (Figure 2). Two commonly used characteristic values of the spectra, the signal intensity of the third harmonic μ_3 and the shape of the spectrum (represented by the ratio of harmonics μ_5/μ_3), discern considerable differences by more than one order of magnitude for the investigated samples ranging from R_{hyd} = 14.7 nm up to 127 nm. The maximum values of about 30 nm were found for R_{hyd} (see inset of Figure 2). Moreover, the resulting signal amplitudes are several orders of magnitude above the noise level which can be attributed to the high specificity of the modality. This allows for the magnetic characterization of highly diluted samples which will be further examined.

Figure 2. MPS batch measurements (B_{exc} = 25 mT, t_{avg} = 1 s) on several different MNP types of the same iron amount (m(Fe) = 280 µg). For simplicity, solely the amplitudes of the odd harmonics are shown. The noise floor of the MPS spectra (marked by a dashed line) was determined by calculating the standard deviation of 20 consecutive measurements of empty PCR tubes. The inset shows the MPS signal dependence (iron normalized third harmonic amplitude μ_3 and shape of the spectrum μ_5/μ_3) on the hydrodynamic size as determined by DLS of the MNPs, showing a maximum at about R_{hyd} = 30 nm.

3.2. Influence of Dilution

Investigation of the linearity of the MPS signal amplitude and the limit of detection (LOD) at a signal-to-noise ratio (SNR) of three was performed using MPS in batch mode (six different MNP samples in PCR tubes; B_{exc} = 25 mT, t_{avg} = 10 s). Therefore, 16 empty PCR tubes were measured to determine the signal variation of the blank, expressed as the standard variation. The measurement results of the MNP dilution series demonstrate a highly linear correlation (R^2 = 0.9997) between the signal amplitude μ_3 and the iron amount m_{Fe} (see Figure 3). The wide dynamic range, e.g., from 780 µg down to 3.3 ng for FER, is of particular note.

Figure 3. MPS batch measurements (B_{exc} = 25 mT, t_{avg} = 10 s) on serial dilutions of MNPs. (**a**) The third harmonic amplitude μ_3 decreases linearly with the decreasing iron amount of the sample. Depending on MNP properties the limit of detection was between 44.5 ng (FM-30) and 3.4 ng (FM-50). Due to the lower variation of the background signal when using a flow cell, the LOD was further reduced by factor of 10. (**b**) The shape of the MPS spectra (μ_5/μ_3) was not affected by dilution with respect to uncertainty. The increasing uncertainties at lower iron concentrations result from the lower signal intensities of μ_5 compared to μ_3, leading to a lower detection limit of μ_5.

Depending on the specified MNP properties, the LOD ranged from 54.7 ng (FM-30) down to 2.2 ng (FM-50). In contrast, the harmonic ratio μ_5/μ_3 was completely unaffected by dilution and enabled the distinction of magnetically different particles down to the LOD of μ_5, ranging from 252 ng for FM-30 down to 5.6 ng for FM-50.

Additionally, a serial dilution of FM-50 was measured using FC2 for comparison with results obtained from standard batch mode measurements. Between each sample measurement the flow cell was not removed or repositioned but cleaned by flushing with ultra pure water. The variation of the background signal of FC2 was therefore measured without removing the cell from the unit between each of 16 measurements, as this corresponds to the use case. When comparing the resulting signal variations, the noise level found for the flow cell measurement was lower by a factor of six. We attribute this to the variability of sample introduction (positioning) and magnetic contaminants of the sample container (PCR tubes) affecting MPS batch mode measurements. Thus, the comparison of dilution series in PCR tubes and FC2 revealed the higher sensitivity of flow cell measurements. The resulting LOD of FM-50 was considerably lower when measured in the flow cell (LOD_{FC2} = 700 pg, LOD_{batch} = 3.4 ng) as can be seen in the inset of Figure 3a. A further important fact is that the measured spectral amplitudes μ_i in batch and flow cell mode coincided perfectly (R^2 = 1).

Note that the lowest iron concentration that can be reliably measured by online MPS also directly depends on the detection volume of the flow cell. Thus, the simple adjustment of detection volume (via the inner diameter of the capillary) allows for the optimization according to desired resolution as well as sensitivity for each experiment.
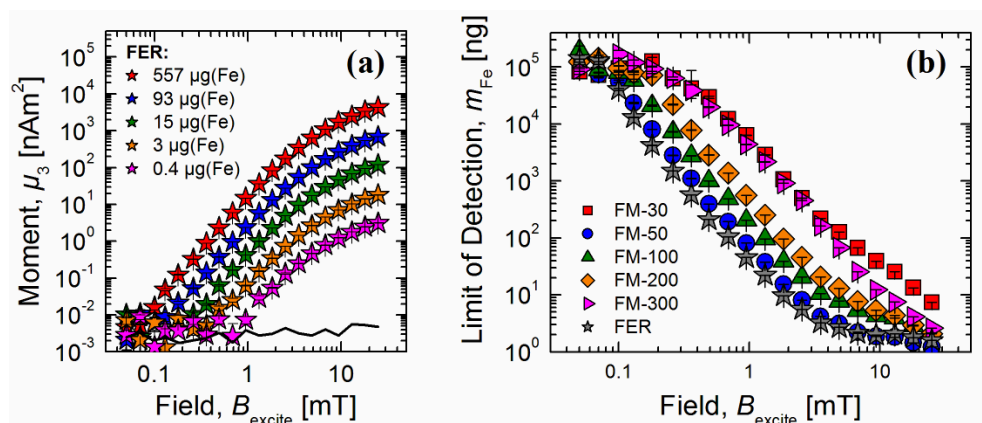
3.3. Influence of Excitation Field

For a more comprehensive study of the magnetic properties of MNPs it is advantageous to apply different excitation fields B_{exc} [17]. Therefore, to test the applicability, the influence of field amplitude
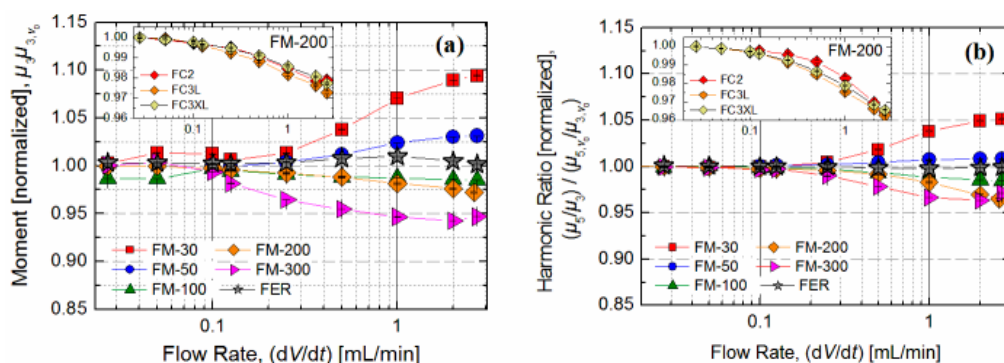
B_{exc} on LOD was studied by measuring MNP-filled PCR tubes from B_{exc} = 0.05 mT up to 25 mT in 20 logarithmic steps each with 20 repetitive measurements (t_{avg} = 1 s). The fluctuation in the background signal, the MPS noise, obtained at each field was quantified by calculating the standard deviation of μ_3 on an empty sample vessel. As the MNP magnetization exhibits a nonlinear behavior, the MPS signal amplitude μ_3 as a function of field amplitude B_{exc} also creates a nonlinear curve as can be seen in Figure 4a for five dilutions of FER. For all MNP samples the LOD was determined for each B_{exc} using the above-mentioned procedure (see Section 3.2). The LOD decreases on average by five orders of magnitude (from approximately 1 mg(Fe) down to 10 ng(Fe)) when the field is increased by at least two orders of magnitude (from 0.1 mT up to 10 mT). Note that all measurements were performed with an averaging time t_{avg} of 1 s which resulted in a 3.16-times higher noise floor compared to 3.2 (measurements performed with t_{avg} = 10 s) due to the proportionality of noise to $(t_{avg})^{0.5}$.

3.4. Influence of Flow Rate

To show the applicability of MPS measurements in continuous flow, the signal dependence of different MNP samples with the same iron concentration (c(Fe) = 279 µg/mL) on nine different flow rates, ranging from 27 µL/min–2.7 mL/min, was determined. For comparison, the signals were normalized to MPS signals obtained at dV/dt = 0 mL/min of the respective samples. Figure 5a shows that changes of the signal amplitude μ_3 due to an increasing flow rate are below 10% for all MNP samples. The largest deviations were found for the smallest and largest particles (R_{hyd} = 14.7 nm and R_{hyd} = 127 nm, respectively) at the highest flow rate of 2.7 mL/min. The μ_5/μ_3 shape factor changed in the same course but was only half as strong as μ_3. In the range of usual operating flow rates for A4F (100 µL/min–1 mL/min) the measured spectra changed less than 7% and 5% for μ_3 and for μ_5/μ_3, respectively. Moreover, the use of different flow cells did not affect the flow-dependent signal change significantly, as can be seen in the insets of Figure 5. To assess the influence of the MPS flow, experiments on MNP size DLS measurements were performed before and after application on sample aliquots. The results obtained confirmed the previous findings as R_{hyd} did not change significantly.

Figure 4. (**a**) The field-dependent MPS signal amplitude μ_3 shown for a serial dilution of FER exhibits a nonlinear curvature. (**b**) This mainly affects the limit of detection which additionally depends on the MPS noise slightly increasing by a factor of three (see (**a**)).

Figure 5. Influence of flow rate on the MPS signal. The changes were evaluated from the ratio of MPS signal (**(a)** μ_3; **(b)** μ_5/μ_3) measured during liquid flow and without flow. **(b)** The insets of **(a)** and **(b)** show the degree of signal change for FM-200 measured in the three different flow cells. No significant variations between the different flow cells were observed.

3.5. MPS Online Detection

Finally, the A4F multidetector platform incorporating UV, DLS, and MALS detection was extended by MPS to demonstrate that the developed MPS online detection is applicable to fractionation experiments. Therefore, the magnetic characterization during fractionation was performed using optimized parameters ($B_{exc} = 25$ mT, $t_{avg} = 10$ s, $dV/dt = 100$ μL/min) gained from preliminary experiments to obtain the highest sensitivity. The hydrodynamic separation was carried out on FER, which is known to have a polydisperse size distribution consisting of single crystallites and clusters [20-23]. Accordingly, this was also confirmed by the measured UV fractogram showing the presence of a bimodal distribution (Figure 6a) exhibiting two distinct maxima with retention coefficients $R = t_0/t_r = 0.5$ and 0.2, respectively. To extract the peak areas of the UV fractogram, a bimodal Gaussian function was used. Consequently, 42% of the eluting species belong to the first population of hydrodynamically small MNPs, whereas 57% can be associated with a second population of larger MNPs, which is in good agreement with experimental data obtained from literature [20]. The calibrated UV signal was further used to determine the iron concentration in the fractions with which the MPS signal amplitudes were normalized.
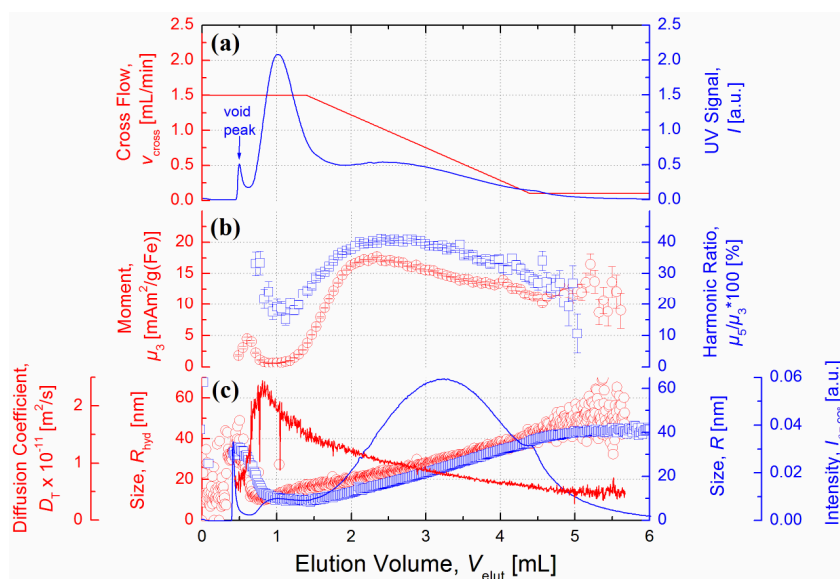
After elution of the void peak, R_{hyd} as well as R increased linearly with V_{elut} as can be seen from the results of particle sizing methods DLS and MALS, respectively (Figure 6c). The smaller and larger population peak have a hydrodynamic size R_{hyd} of about 13 nm and 25 nm, respectively. Notably, R_{hyd} of the large population is nearly equal to the value obtained for the initial state of FER (see Table 1) which highlights the underestimation of small species using DLS in batch mode. In addition to R_{hyd}, the radii obtained by MALS are shown in Figure 6c. As the MALS contribution of the stabilizing carboxydextran shell is negligible, R is significantly smaller than R_{hyd} at any point during fractionation. Thus, a mean shell thickness of about 7 nm can be derived.

The magnetically characteristic signature of the eluting MNPs represented by μ_3 and the μ_5/μ_3 ratio was strongly affected by the hydrodynamic splitting of FER as measured by MPS online detection. To avoid misinterpretation, signals below an SNR of three are not shown in Figure 6b. To ensure comparability, concentration-dependent μ_3 values were divided by respective iron amounts. As can be seen in Figure 6b, MPS spectra of the smaller population peak have considerably lower signal amplitudes ($\mu_3 \sim 0.7$ mAm^2/g(Fe)) and a steeper decay ($\mu_5/\mu_3 \sim 15\%$) compared to the larger population. These results

are in line with the data obtained by MPS batch mode measurements reported in Section *3.2* (Figure 2) showing that MNPs of similar hydrodynamic size (FM-30: R_{hyd} = 13.7 nm) were characterized by a μ_5/μ_3 ratio of about 13% and an iron normalized signal amplitude of about 0.7 mAm^2/g(Fe). Whereas the maximum signal amplitude $\mu_3 \sim$ 18 mAm2/g(Fe) of the second MNP population (at a size of R = 15.7 nm and R_{hyd} = 22 nm) is a factor of 2.2 higher compared to unfractionated FER, the μ_5/μ_3 ratio improved only slightly from 39% to 41%. Nevertheless, these values are in very good agreement with previous measurements on separated FER using MPS in batch mode [23]. For even later elution times, *i.e.*, lager sizes, both μ_3 as well as μ_5/μ_3 again decreased.

This nonlinear MPS signal dependence on MNP size is in accordance with observations in Section *3.2* and other studies [27]. It was experimentally shown that narrowly distributed single-core MNPs of R = 10 nm and R_{hyd} = 15 nm yield the highest MPS signal intensity. These values are only slightly smaller compared to ours obtained from fractionation of FER which, on the contrary, consists of clusters of small primary particles (thus called multi-core) MNPs. The size-dependent optimum in MPS signal is known to be caused by magnetic relaxation effects increasing with MNP size.

The first considerably smaller peak located at the void peak can be explained by pre-elution of partially unretained MNPs caused by repulsion between MNPs and the membrane surface.

Figure 6. (**a**) A linear decay of V_x (red line) from 1.5 mL/min to 0.1 mL/min was applied at V_{Ch} = 0.5 mL/min, resulting in an enforced elution of hydrodynamically larger MNPs. The A4F fractogram of FER with UV detection at λ = 280 nm (blue line) exhibits a double-peak indicating the existence of two distinct hydrodynamic size modes. (**b**) Characteristic MPS signal parameter μ_3 (red circles) and the μ_5/μ_3 ratio (blue squares) were characterized by a nonlinear correlation to the determined sizes, reaching a maximum at about 21 nm and 15 nm for R_{hyd} and R, respectively. Values below the noise floor are not shown. (**c**) The sizes determined by DLS (red circles) and MALS (blue squares) showed a linear increase from 10 nm up to 45 nm and 9 nm up to 41 nm for R_{hyd} and R, respectively. The corresponding diffusion coefficient determined by DLS (red line) strongly decreases from V_{elut} = 0.8 mL to 5.5 mL by a factor of five. The light scattering intensity (detected at θ = 92°) shows a maximum at V_{elut} = 3.3 mL.

4. Summary and Conclusions

The primary features of the magnetic characterization using MPS are its specificity, high sensitivity, and wide linear dynamic range down to few nanogram of iron. The comparison of colloidally stable MNP fluids with the same iron content showed the MPS sensitivity may differ more than one order of magnitude for different MNP compositions. Furthermore, technical parameters such as the excitation field amplitude as well as the averaging time have a strong impact on sensitivity and thus on the applicability for A4F.

To enable MPS online detection we developed flow cells based on a coiled capillary. The construction allows for the adjustment of different detector volumes to optimize the setup regarding resolution and sensitivity. Continuous flow experiments using the novel flow cells revealed that increasing flow rates may have a significant impact on the MPS signal which appears to be MNP size-dependent. Nevertheless, for usual flow rates (100 µL/min–1 mL/min) used for A4F, the MPS signal change was below 7%.

Finally, the first-time integration of an MPS device into an A4F multidetector platform was successfully achieved and the suitability was demonstrated by the hydrodynamic separation of a commercial MRI contrast agent. The MPS online detection revealed a nonlinear MPS signal dependence from the MNP size which was determined by DLS and MALS. Therefore, by hyphenation of the established chromatographic A4F technique with the outstanding magnetic measurement tool MPS, a powerful new analysis platform is supplied which may shed light on important insights in the physics of MNPs and can be used as a standard analytical method for quality control of MNPs in biomedical applications.

Acknowledgments

Author Contributions

Norbert Löwa developed the concept for the flow cells, performed measurements, data analysis, and drafted the manuscript. Dirk Gutkelch and Rinaldo August were responsible for realization and refinement of the flow cell concept. Patricia Radon performed MPS measurements and analysis and contributed to the manuscript. Frank Wiekhorst contributed substantially to the design of the study and the production of the manuscript.

Conflicts of Interest

The authors declare no conflict of interest.

References

1. Goya, G.F.; Grazu, V.; Ibarra, M.R. Magnetic nanoparticles for cancer therapy. *Curr. Nanosci.* **2008**, *4*, 1–16.
2. Pankhurst, Q.A.; Connolly, J.; Jones, S.K. Applications of magnetic nanoparticles in biomedicine. *J. Phys. D* **2003**, *36*, R167.
3. Ittrich, H.; Peldschus, K.; Raabe, N.; Kaul, M.; Adam, G. Superparamagnetic iron oxide nanoparticles in biomedicine: Applications and developments in diagnostics and therapy. *Rofo* **2013**, *185*, 1149–1166.
4. Dennis, C.L.; Krycka, L.K.; Borchers, J.A.; Desautels, R.D.; van Lierop, J.; Huls, N.F.; Jackson, J.; Gruettner, C.; Ivkov, R. Internal magnetic structure of nanoparticles dominates time-dependent relaxation processes in a magnetic field. *Adv. Funct. Mater.* **2015**, *25*, 4300–4311.
5. Yu, S.S.; Lau, C.M.; Thomas, S.N.; Jerome, W.G.; Maron, D.J.; Dickerson, J.H.; Hubbel, J.A.; Giogio, T.D. Size-and charge-dependent non-specific uptake of PEGylated nanoparticles by macrophages. *Int. J. Nanomed.* **2012**, *7*, 799.
6. Huang, J.; Bu, L.; Xie, J.; Chen, K.; Cheng, Z.; Li, X.; Chen, X. Effects of nanoparticle size on cellular uptake and liver MRI with polyvinylpyrrolidone-coated iron oxide nanoparticles. *ACS Nano* **2010**, *4*, 7151–7160.
7. Willard, M.A.; Kurihara, L.K.; Carpenter, E.E.; Calvin, S.; Harris, V.G. Chemically prepared magnetic nanoparticles. *Int. Mater. Rev.* **2004**, *49*, 125–170.
8. Kratz, H.; Eberbeck, D.; Wagner, S.; Taupitz, M.; Schnorr, J. Synthetic routes to magnetic nanoparticles for MPI. *Biomed. Biomed. Eng.* **2013**, *58*, 509–515.
9. Luigjes, B.; Woudenberg, S.M.; de Groot, R.; Meeldijk, J.D.; Torres Galvis, H.M.; de Jong, K.P.; Philipse, A.P.; Erné, B.H. Diverging geometric and magnetic size distributions of iron oxide nanocrystals. *J. Phys. Chem. C* **2011**, *115*, 14598–14605.
10. Janca, J. *Field-Flow Fractionation: Analysis of Macromolecules and Particles*; M. Dekker Inc: New York, NY, USA, 1988; pp. 1–336.
11. Lespes, G.; Gigault, J. Hyphenated analytical techniques for multidimensional characterisation of submicron particles: A review. *Anal. Chim. Acta* **2011**, *692*, 26–41.
12. Gleich, B.; Weizenecker, J. Tomographic imaging using the nonlinear response of magnetic particles. *Nature* **2005**, *435*, 1214–1217.
13. Weizenecker, J.; Gleich, B.; Rahmer, J.; Borgert, J. Micro-magnetic simulation study on the magnetic particle imaging performance of anisotropic mono-domain particles. *Phys. Med. Biol.* **2012**, *57*, 7317.
14. Ludwig, F.; Remmer, H.; Kuhlmann, C.; Wawrzik, T.; Arami, H.; Ferguson, R.M.; Krishnan, K.M. Self-consistent magnetic properties of magnetite tracers optimized for magnetic particle imaging measured by ac susceptometry, magnetorelaxometry and magnetic particle spectroscopy. *J. Magnet. Magnet. Mater.* **2014**, *360*, 169–173.
15. Graeser, M.; Bente, K.; Buzug, T.M. Dynamic single-domain particle model for magnetite particles with combined crystalline and shape anisotropy. *J. Phys. D* **2015**, *48*, 275001.

16. Wawrzik, T.; Yoshida, T.; Schilling, M.; Ludwig, F. Debye-based frequency-domain magnetization model for magnetic nanoparticles in magnetic particle spectroscopy. *IEEE Trans. Magnet.* **2015**, *51*, 1–4.

17. Deissler, R.J.; Wu, Y.; Martens, M.A. Dependence of Brownian and Néel relaxation times on magnetic field strength. *Med. Phys.* **2014**, *41*, 012301.

18. Wawrzik, T.; Ludwig, F.; Schilling, M. Multivariate magnetic particle spectroscopy for magnetic nanoparticle characterization. *AIP Conference Proceedings* **2010**, *1311*, 267–270.

19. Dutz, S.; Kuntsche, J.; Eberbeck, D.; Müller, R.; Zeisberger, M.. Asymmetric flow field-flow fractionation of superferrimagnetic iron oxide multicore nanoparticles. *Nanotechnology* **2012**, *23*, 355701.

20. Thünemann, A.F.; Rolf, S.; Knappe, P.; Weidner, S. In situ analysis of a bimodal size distribution of superparamagnetic nanoparticles. *Anal. Chem.* **2008**, *81*, 296-301.

21. Lohrke, J. Herstellung und Charakterisierung neuer nanopartikulärer SPIO-Kontrastmittel für die Magnetresonanztomographie. Ph.D. Thesis, University of Halle, Faculty of Natural Science, 2010.

22. Löwa, N.; Knappe, P.; Wiekhorst, F.; Eberbeck, D.; Thünemann, A.F.; Trahms, L. Hydrodynamic and magnetic fractionation of superparamagnetic nanoparticles for magnetic particle imaging. *J. Magnet. Magnet. Mater.* **2015**, *380*, 266–270.

23. Löwa, N.; Knappe, P.; Wiekhorst, F.; Eberbeck, D.; Thunemann, A.F.; Trahms, L. How Hydrodynamic Fractionation Influences MPI Performance of Resovist. *IEEE Trans. Magnet.* **2015**, *51*, 1–4.

24. Berkov, D.V.; Görnert, P.; Buske, N.; Gansau, C.; Mueller, J.; Giersig, M.; Neumann, W; Su, D. New method for the determination of the particle magnetic moment distribution in a ferrofluid. *J. Phys. D* **2000**, *33*, 1–7.

25. Eberbeck, D.; Wiekhorst, F.; Wagner, S.; Trahms, L. How the size distribution of magnetic nanoparticles determines their magnetic particle imaging performance. *Appl. Phys. Lett.* **2011**, *98*, 182502.

26. Snyder, S.R.; Heinen, U. Characterization of magnetic nanoparticles for therapy and diagnostics. Bruker BioSpin: Ettlingen, Germany, 2010. Available online: https://www.bruker.com/fileadmin/user_upload/8-PDF-docs/MagneticResonance/MRI/brochures/MPS_app-note.pdf (accessed on 31 July 2015).

27. Ferguson, M.R.; Khandhar, A.P.; Krishnan, K.M. Tracer design for magnetic particle imaging (invited). *J. Appl. Phys.* **2012**, *111*, 07B318.